

Supplemental Information

This supplemental information contains technical information about the analyses presented in the main paper.

Participant MRI

The participants in the study had a structural MRI. The MRI data were collected on a; and other details of the structural MRI, T1W and T2W. The scans had 1 mm³ resolution and sufficient FoV to cover from the top of the head down to the neck

Localization of External Fiducials and Electrode Fiducials

A Polhemus digitizer was used to locate in 3D space external scalp fiducial points and electrode fiducial points. The scalp fiducials were a set of external head locations used for the 10-10 system (Nz, Iz, LMA, RMA, LPA, RPA, Vz). These were digitized and the 3D coordinates saved. We also digitized the location of some “electrode fiducials” for the electrode generation. These were located on the Hydrocel Geodesic Sensor Net 128 (HGSN128) net near the fiducials (Nz-17, Oz-75, LMA-57, RMA-100, LPA-44, RPA-115, Vz-129).

External head measurements were done on each participant. The measures include semi-circumferences (front and rear sides-circumference from LMA to RMA, top circumferences from Nz to Iz, and from LMA to RMA) and lateral diameters (Nz to Iz, LMA to RMA).

Electrode Locations on MRI

The MRICron program (Rorden, <http://www.mccauslandcenter.sc.edu/mricro/mricron/>) was used to display MRIs and do editing work. A set of fiducials were located on each MRI, including the anterior commissure, posterior commissure and a set of external head locations

used for the 10-10 system (e.g., Nz, Iz, LMA, RMA, LPA, RPA, Vz). These locations were identical to the ones measured with the digitizer.

Average electrode placement locations were available that were constructed on age-appropriate average MRI template from the Neurodevelopmental MRI database (Richards et al., 2015a; Richards & Xie, 2015). The average electrodes were constructed from individual participants who had the positions of the HGSN 128 channel electrode net determined on the head. The electrode positions on the individuals were transformed to the average MRI template and averaged, and fitted to the average MRI template (Richards, 2015; Richards et al., 2015b).

The average electrode placements locations were transformed into the individual participant locations with the help of the external scalp fiducials and electrode fiducials. First, the digitized scalp fiducials were registered to the MRI scalp fiducials using “coherent point drift” registration (CPD version 2; Myronenko et al, 2006; Myronenko & Song, 2010). The resulting 12-degree of freedom affine registration matrix was used to transform the digitized electrode fiducials into the MRI space, thus giving the locations of the actual fiducial electrodes for each participant in MRI space. Second, the digitized-transformed electrode fiducial locations were then registered to the same electrodes on the age-appropriate average electrode placements with CPD. The registration matrix was then used to transform the average electrode placements into the participant space. This transformed electrode configuration was then fitted to the scalp by finding the nearest location to the scalp from the electrode. The resulting electrode locations were referenced to the AC-coordinate system for that participant. The CPD registration / transformation resulted in the digitized and transformed electrode fiducials being nearly in the exact same space, and presumably the average electrode configuration also was placed in the

appropriate space with this method (see Richards, 2015, and Richards et al., 2015a for details of these procedures).

Supplemental Information in Richards (2013)

We rely on methods presented in Richards (2013), both the main text and the supplemental information for that study. The following sections include details found either in the Supplemental Information or the main paper for that study.

Head Segmentation The materials in the head were segmented, including scalp, skull, CSF, white matter, gray matter, nasal cavity, and eyes (Richards, 2002, 2005, 2013). The gray matter was used as the source volume for the analysis.

Atlases Three atlases were constructed on the individual participants MRIs. The LONI Probabilistic Brain Atlas (LPBA40; Shattuck, et al., 2008) and the Hammers atlas, based on MRIs from the Information Exchange for the Internet (Hammers atlas; Heckemann, Hajnal, Aljabar, Rueckert, & Hammers, 2006; Heckemann, et al., 2003) were constructed on individual participants. Details of the construction of these atlases for individual participants may be found in Phillips et al. (2012) and Fillmore et al. (2015); and we have used these atlases in previous work to define ROIs for cortical source analysis (Guy, Zieber, & Richards, 2015; Richards, 2013; Xie & Richards, 2015; also see Supplemental Information for Richards, 2013). The LPBA40 atlas has 56 areas defined for the cortex, sub-cortex, brainstem, and cerebellum. The Hammers atlas has 83 areas defined from the cortex, sub-cortex, brainstem, and cerebellum. The third atlas was an automatically constructed lobar atlas that defined the major lobes (e.g., frontal, temporal) of the cortex, some sub-lobar cortical areas (e.g., fusiform gyrus), subcortical (e.g., striatum, thalamus), cerebellum and brainstem. This atlas was constructed from a manually-labeled age-appropriate lobar atlas transformed into the participant's MRI space, the adult MRI average

template lobar atlas transformed into the participant space, and the relevant segments from the LPBA and Hammers atlas. These atlases were combined with a majority vote procedure to define a lobar atlas for each individual MRI.

We also used two atlases based on an age-appropriate atlas for each participants. The “Harvard-Oxford” (cite) and Brodmann (cite) atlases were used from the FSL computer program. These atlases were transformed from the MNI152 atlas used in the FSL computer program to age-appropriate atlases. This atlas, now in the age-appropriate template space, was further transformed into the participant space.

The atlases were used to define several anatomical areas by identifying common designations from each of the atlases, and ROIs were mapped for each participant MRI. These ROIs are listed in the main paper, and show in Figure 1 of the main paper. They were chosen based on theoretical grounds or previous research examining ERN components brain areas in adult participants. The primary ones of interest were the orbital-frontal gyrus, ventral anterior cingulate, dorsal anterior cingulate, and ventral-lateral inferior frontal gyrus. Additionally, we used other ROIs that could account for ERP activity that might not be specifically related to the ERN effects. These include the parietal lobe, intraparietal sulcus, frontal pole, dorsolateral prefrontal cortex, and motor and premotor areas. Supplemental Information Table 2 has a list of the ROIs The label in that table are for the anatomical areas taken from the lobar, Hammers, LPBA40, or Harvard-Oxford atlas, or are the Brodmann areas.

EMSE Source analysis Source analysis was conducted with realistic head models and the current density reconstruction (CDR) technique to determine the cortical activity in the ROIs. This was done both with the EMSE’s Data Analysis module (Source Signal) and the Fieldtrip computer program. First, the electrode locations, source locations, and head

model generated in the previous procedures were used with EMSE's Data Analysis (Source Signal, Inc) to estimate the forward model and inverse model. The realistic cortical source models used an FEM mapping of the electrical conductivity of the head to calculate the forward model. The forward model was used to estimate a lead-field matrix. This lead-field matrix estimation was based on the locations of the electrodes on the scalp, the source locations defined by the segmented GM and the location of the eyes, and the FEM model for the individual participant. Second, cortical activity was estimated as the current source density of cortical source locations with the CDR technique and the sLORETA (Pascual-Marqui, 2002; Pascual-Marqui, Michel, & Lehmann, 1994) as the constraint for the CDR. The ERP data surrounding the N1 and ERN peaks was used to estimate the CDR volumes. The resulting values were a source map of amplitude vectors (CDR moments) that was transformed into a power value. Thus for every cortical source location there was a current density at that location, the sum of which would generate the scalp-recorded EEG.

Fieldtrip Source Analysis

The Fieldtrip (citation) computer programs were used for source analysis. The FT programs are a set of procedures for MATLAB that do segmentation, head model generation, and source analysis. They use both custom programs and integrate MRI programs from other sources (e.g., SPM, BESA, FreeSurfer). The following steps were used to generate the head models and do the source analysis. Custom MATLAB macros were used in each step that took account of the computer-storage organization of the author; however a brief min-script for each FT call is presented.

1—Create a MRI information file. The first step was to create a information file describing the MRI. This was used for some of the programs, and to align the MRI space into AC-defined

space (ft_volumerealign). The file saved the AC, PC, external scalp fiducials, and the MRI dimensions. (i.e., mrinfo structure with ac, pc, nz, iz, xdim, ydim, zdim).

2—Electrode files. The electrode placement files were read from the placement locations above and save in the FT format (i.e., a elec structure, with elecpos, chanpos, unit, label).

3—Source grid files. The The gray matter segmentation was used to construct the locations of sources for the current density reconstruction. The gray matter segmentation was used to construct the locations of sources for the current density reconstruction. The eyes were also included (cf. Richards, 2015, adolescents). This was done by loading the gray matter partial volume estimates, and the segmented eyes locations, and aligning the volume to the AC-defined space (ft_volumerealign). A 3mm grid was then created from the resulting MRI volume (ft_prepare_sourcemodel, ft_determine_coordsys). The grid positions (grid.pos) were then used to map to the coordinates of a MRI and this MRI was also saved. We also created a 1mm grid for each participant and a 1mm MRI of the source locations. Figure nn shows the grid with the electrodes plotted about the grid positions.

4—Head models. We created both Boundary Element Method (BEM) and Finite Element Method (FEM) head models. These were done from the segmentation of the MRI. For the BEM model, the outer scalp, skull, CSF, and brain were constructed into a 4-compartment MRI. The compartments were modified slightly so each inner compartment was contained in all the outer compartments (scalp skull CSF brain) and this volume was realigned to the AC-defined space (ft_volumerealign). A mesh was created for each compartment using “projectmesh” and 2000 vertices (ft_prepare_mesh). Figure nn shows the resulting mesh plotted with the electrodes on the edges of the mesh. The four meshes, conductivity, and tissue names were then used to create a “DIPOLI” (citation) BEM model (ft_prepare_headmodel). For the FEM model, the full

segmented head was used. The tissue types

({'wm','gm','t2wcsrf','dura','skull','scalp','head','eyes','nasalcavity'}) and the MRI voxel values were loaded into a FT MRI volume, and aligned to the AC-defined space (ft_volumerealign).

The head model was used to create a wireframe mesh with hexahedral

volumes.(ft_prepare_mesh). The mesh and conductivity values were used to create a “SIMBIO” (citation) FEM model (ft_prepare_headmodel).

5—Lead-field matrices. The leadfield matrices were created with electrodes, source model, and head model (ft_prepare_leadfield).. A leadfield matrix was created for each model (BEM-DIPOLI, FEM-SIMBIO).

6—Source reconstruction—CDR reconstructions The source reconstructions were done with exact-LORETA (eLORETA). The lead field matrices exist for BEM and FEM models, and each with a eLORETA source reconstruction. The leadfield matrices and ERP data files are loaded and the source reconstruction is done (ft_sourceanalysis). The resulting amplitude vector (CDR moment) was transformed into a power value. Thus for every location in the source model grid a power value was obtained representing the current density at that location needed to generate the scalp ERP (given the head model and source inverse restraint).

Anatomical ROIs and CDR-per-mm in ROI, and Estimated MRI Volumes

The source reconstructions from both EMSE and Fieldtrip were used to get the sum (and mean)

CDR per mm for each ROI. The MRI segmented anatomical atlases were transformed from

segmented MRI volumes into a series matrix values for the segmented atlas voxel type and atlas

position. The segmented atlas positions were then used to identify each position in the CDR

matrix, and sum the CDR values across the entire ROI. The mean CDR per mm was computed

as the summed CDR divided by the number of grid points making up that atlas segment. Thus for

each msec of the ERP data put into the model, we have the CDR values for each ROI in our atlas segments.

In addition to the CDR values for each atlas ROI segment, I also created a simulated MRI volume based on the CDR values. This was done with the `fit_sourceinterpolate` programs. This program maps the grid position of each CDR value into the coordinates of a MRI and assigning the voxel value as the CDR value for that grid position. This was done for the original resolution (3mm), and also for an interpolated 1mm MRI volume using spline interpolation.

References

- Fillmore, P., Richards, J. E., Phillips-Meek, M. C., Connington, A. & Stevens, M (2014a). *Stereotaxic MRI brain atlases for infants from 3 to 12 months*.
- Hamalainen, J. A., Ortiz-Mantilla, S., & Benasich, A. A. (2011). Source localization of event-related potentials to pitch change mapped onto age-appropriate MRIs at 6 months of age. *Neuroimage*, *54*(3), 1910-1918. doi: 10.1016/j.neuroimage.2010.10.016
- Hammers, A., Allom, R., Koepp, M. J., Free, S. L., Myers, R., Lemieux, L., . . . Duncan, J. S. (2003). Three-dimensional maximum probability atlas of the human brain, with particular reference to the temporal lobe. *Hum Brain Mapp*, *19*(4), 224-247. doi: 10.1002/hbm.10123
- Heckemann, R. A., Hajnal, J. V., Aljabar, P., Rueckert, D., & Hammers, A. (2006). Automatic anatomical brain MRI segmentation combining label propagation and decision fusion. *Neuroimage*, *33*(1), 115-126. doi: 10.1016/j.neuroimage.2006.05.061
- Heckemann RA, H. T., Leung K, Hill DLG, Hajnal JV, Rueckert D. (2003). *Information Extraction from Medical Images (IXI): Developing an e-Science Application Based on the Globus Toolkit*. Nottingham, UK.
- McCleery, J. P., & Richards, J.E. (April, 2012). *Comparing realistic head models for cortical source locationization of infant event-related potentials*. . Paper presented at the Poster presented at the 3rd UK Paediatric Neuropsychology Symposium, University College London Institute for Child Health, London, England.
- McCleery, J. P., & Richards, J.E. (June, 2012). *Comparing realistic head models for cortical source locationization of infant event-related potentials*. . Paper presented at the International Conference on Infant Studies, , Minneapolis, MN.
- Myronenko, A., Song, X., & Carreira-Perpinan, M. (2007). Non-rigid point set registration: Coherent point drift. . *Advances in Neural Information Processing Systems -- Proceedings of the 2006 Conference.*, *19*, 1009-1016.
- Myronenko, A., & Song, X. . (2010). Point Set Registration: Coherent Point Drift. *IEEE Transactions on Pattern Analysis and Machine Intelligence.*, *32*, 2262-2275.
- Ortiz-Mantilla, S., Hamalainen, J. A., & Benasich, A. A. (2012). Time course of ERP generators to syllables in infants: a source localization study using age-appropriate brain templates. *Neuroimage*, *59*(4), 3275-3287. doi: 10.1016/j.neuroimage.2011.11.048
- Phillips, M. C., Richards, J. E., Stevens, M. & Connington, A. . (2013). *A stereotaxic MRI brain atlas for infant participants*. Paper presented at the Society for Research in Child Development, Seattle, WA.
- Reynolds, G. D., Courage, M. L., & Richards, J. E. (2010). Infant attention and visual preferences: converging evidence from behavior, event-related potentials, and cortical source localization. *Dev Psychol*, *46*(4), 886-904. doi: 10.1037/a0019670
- Reynolds, G. D., & Richards, J. E. (2005). Familiarization, attention, and recognition memory in infancy: an event-related potential and cortical source localization study. *Dev Psychol*, *41*(4), 598-615. doi: 10.1037/0012-1649.41.4.598
- Reynolds, G. D., & Richards, J. E. (2009). Cortical source localization of infant cognition. *Dev Neuropsychol*, *34*(3), 312-329. doi: 10.1080/87565640902801890
- Richards, J. E. (2002). *Using EMSE and EGI for source analysis display and illustration*. Retrieved from <http://jerlab.psych.sc.edu/pdf/emseegi.pdf>

- Richards, J. E. (2006). *Realistic cortical source models of ERP*. Retrieved from <http://jerlab.psych.sc.edu/PDF%20Files/RealisticSourceModels.pdf>
- Richards, J. E. (2013). Cortical sources of ERP in prosaccade and antisaccade eye movements using realistic source models. *Front Syst Neurosci*, 7, 27. doi: 10.3389/fnsys.2013.00027
- Richards, J. E., Boswell, C., Stevens, M., & Vendemia, J. M. (2015). Evaluating methods for constructing average high-density electrode positions. *Brain Topogr*, 28(1), 70-86. doi: 10.1007/s10548-014-0400-8
- Richards, J. E., Sanchez, C., Phillips-Meek, M., & Xie, W. (2015). A database of age-appropriate average MRI templates. *Neuroimage*. doi: 10.1016/j.neuroimage.2015.04.055
- Richards, J. E. X., W. (2015). Brains for all the ages: Structural neurodevelopment in infants and children from a life-span perspective. In J. Bensen (Ed.), *Advances in Child Development and Behavior* (Vol. 48).
- Sanchez, C. E., Richards, J. E., & Almli, C. R. (2011). Neurodevelopmental MRI brain templates for children from 2 weeks to 4 years of age. *Dev Psychobiol*, 54(1), 77-91. doi: 10.1002/dev.20579
- Shattuck, D. W., Mirza, M., Adisetiyo, V., Hojatkashani, C., Salamon, G., Narr, K. L., . . . Toga, A. W. (2008). Construction of a 3D probabilistic atlas of human cortical structures. *Neuroimage*, 39(3), 1064-1080. doi: 10.1016/j.neuroimage.2007.09.031

Fieldtrip Macros

Realign MRI volumes to AC-defined space

```
cfg=[];
cfg.method='fiducial';
cfg.landmark.ac=mriinfo.ac;
cfg.landmark.pc=mriinfo.pc;
cfg.landmark.xzpoint=mriinfo.vertex;
cfg.landmark.right=mriinfo.rpa;
cfg.coordsys='spm';
cfg.parameter='gray';
mri=ft_volumerealign(cfg,mri);
```

Create the source model grid

```
cfg=[];
cfg.mri=mri;
cfg.threshold=.25;
cfg.smooth='no';
cfg.elec=elec;
cfg.grid.resolution=mmresol; % 1 mm or 3 mm
cfg.grid.unit='mm';
grid = ft_prepare_sourcemodel(cfg,mri);
grid=ft_determine_coordsys(grid,'interactive','no')
```

Create a compartment volume mesh

```
cfg = [];
cfg.method = 'projectmesh';
cfg.tissue = 'gray';
cfg.numvertices = 2000;
mesh = ft_prepare_mesh(cfg, mri);
```

Prepare the BEM-DIPOLI head model

```
cfg          = [];
cfg.feedback = false;
cfg.method    = 'dipoli';
cfg.isolatedsource = 'no';
cfg.conductivity = [conductivity(6) conductivity(5) conductivity(3) conductivity(2)]
cfg.tissue      = {'scalp','skull','csf','gray'};
vol            = ft_prepare_headmodel(cfg,mesh);
```

Prepare the FEM mesh

```
cfg = [];
cfg.shift = 0.3;
cfg.method = 'hexahedral';
mesh = ft_prepare_mesh(cfg,mri);
```

Prepate the BEM-SIMBIO head model

```
cfg = [];  
cfg.method='simbio';  
cfg.conductivity=conductivity;  
vol = ft_prepare_headmodel(cfg, mesh);
```

Prepare the lead-field matrix

```
cfg=[]  
cfg.vol=vol;  
cfg.elec=elec;  
cfg.grid=grid;  
cfg.normalize='no';  
lf=ft_prepare_leadfield(cfg);
```

MNE Source reconstruction

```
cfg=[];  
cfg.method='mne';  
cfg.vol=vol;  
cfg.elec=elec;  
cfg.grid=lf;  
cfg.projectnoise='yes';  
cfg.keepcsd='yes';  
cfg.mne.projectnoise='yes';  
cfg.mne.keepcsd='yes';  
cfg.mne.lambda=.000001;;  
cfg.mne.prewhten='no';  
sourcemne=ft_sourceanalysis(cfg,ERPdata);
```

eLORETA source reconstruction

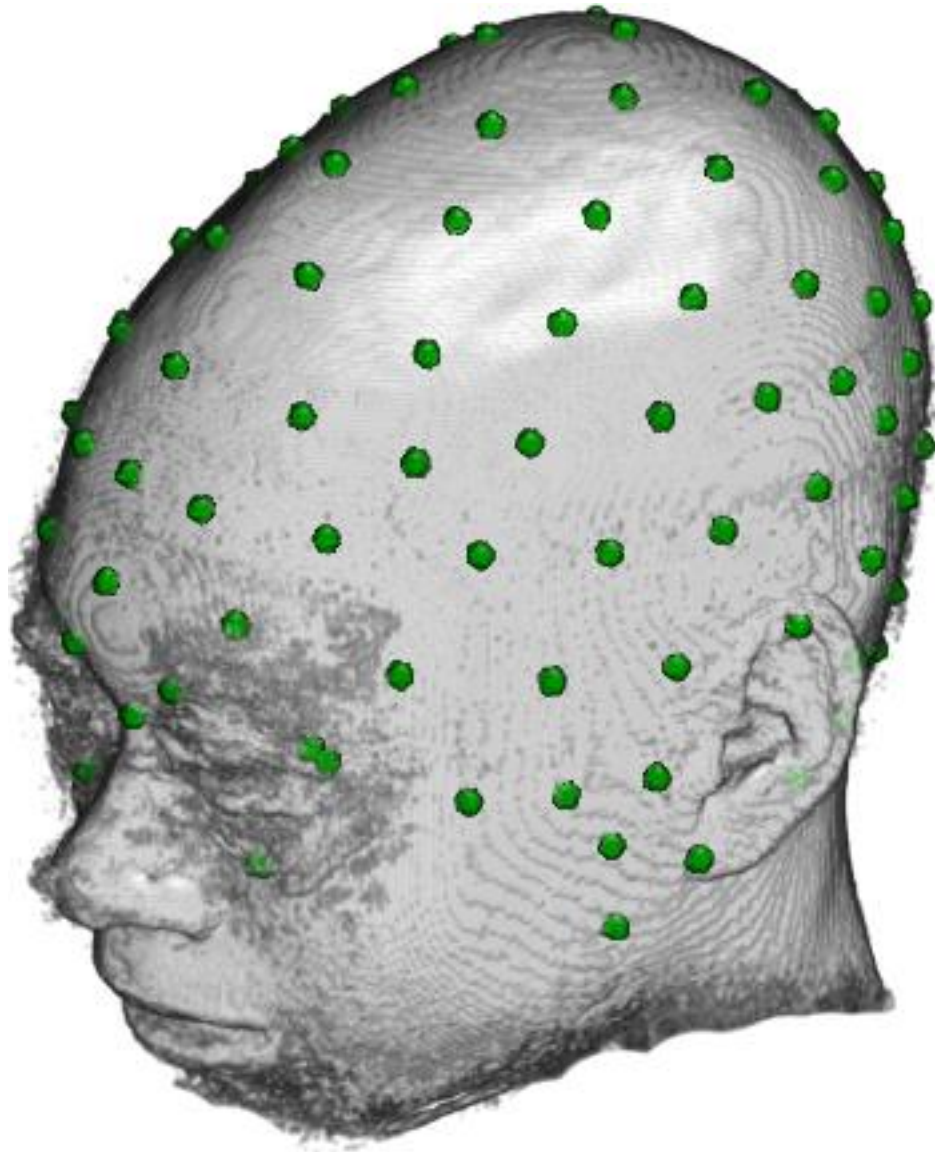
```
cfg=[];  
cfg.method='eloreta';  
cfg.vol=vol;  
cfg.elec=elec;  
cfg.grid=lf;  
cfg.projectnoise='yes';  
cfg.keepcsd='yes';  
cfg.eloreta.projectnoise='yes';  
cfg.eloreta.keepcsd='yes';  
cfg.eloreta.keepmom='yes';  
cfg.eloreta.lambda=1e-5;  
cfg.lambda=cfg.eloreta.lambda;  
sourceft=ft_sourceanalysis(cfg,centermean);
```

Table 2. Regions-of-interest (ROIs) and anatomical regions with labels from the lobar, Hammers, LPBA40, Harvard-Oxford, and Brodman atlases. The left column are lateralized, and are presented from posterior-anterior and lateral-medial. The right column are bilateral and presented from posterior to anterior.

Lateral inferior frontal gyrus		Frontal pole	
LPBA40		Harvard-Oxford	Frontal pole
25, 26	Inferior frontal gyrus (L,R)	Orbito-frontal gyrus	
Hammers		LPBA40	
56, 57	Inferior frontal gyrus (L,R)	29,30	Middle orbitofrontal gyrus
Brodman		33,34	Gyrus rectus
47	Inferior frontal gyrus	Hammers	
Insula		53, 53	Straight gyrus
Insula		68,69	Medial orbital gyrus
Lobar	Insula	Ventral anterior cingulate cortex (Anterior to AC, superior to mid-corpus callosum)	
LBPA40		LPBA40	
101,102	Insular cortex (L,R)	121,122	Cingulate gyrus
Hammers		Hammers	
20,21	Insula (L,R)	76,77	Subgenual anterior cingulate
Dorsolateral prefrontal cortex		78,79	Subcallosal area
Brodman		80,81	Pre-subgenual anterior cingulate
9, 46	Dorsolateral prefrontal cortex	24,25	Cingulate gyrus, anterior (supragenual)
Frontal eye fields		Harvard-Oxford	Paracingulate gyrus
Brodman		Dorsal anterior cingulate cortex (Anterior to AC, superior to mid-corpus callosum)	
6, 8	Premotor, frontal eye fields	LPBA40	
Precentral and postcentral gyrus		121,122	Cingulate gyrus
LPBA40		Hammers	
27,28	Precentral gyrus (L,R)	24,24	Cingulate gyrus, anterior (supragenual)
41,42	Postcentral gyrus (L,R)	Posterior cingulate cortex (Posterior to AC)	
Hammers		LBPA40	
50,51	Precentral gyrus (L,R)	121,122	Cingulate gyrus
60,61	Postcentral gyrus (L,R)	Hammers	
Superior parietal lobe		26, 27	Cingulate gyrus, posterior part
LPBA40			
43,44	Superior parietal gyrus(L,R)		
Hammers			
62,63	Superior parietal gyrus(L,R)		
Supramarginal gyrus			
LPBA40			
45,46	Supramarginal gyrus (L,R)		
Angular gyrus			
LPBA40			
47,47	Angular gyrus		
Intraparietal sulcus			
3mm border between inferior parietal lobe (LPBA40 SMG, AG; Hammers Remainder of parietal cortex) and superior parietal lobe (LPBA40 and Hammers)			

Figure 1. Hydrocel GSN 128 electrode positions on the structural MRI of a 14-year-old participant and the 14-year-old average MRI template

14-Year-Old Participant



14 Years Average MRI Template

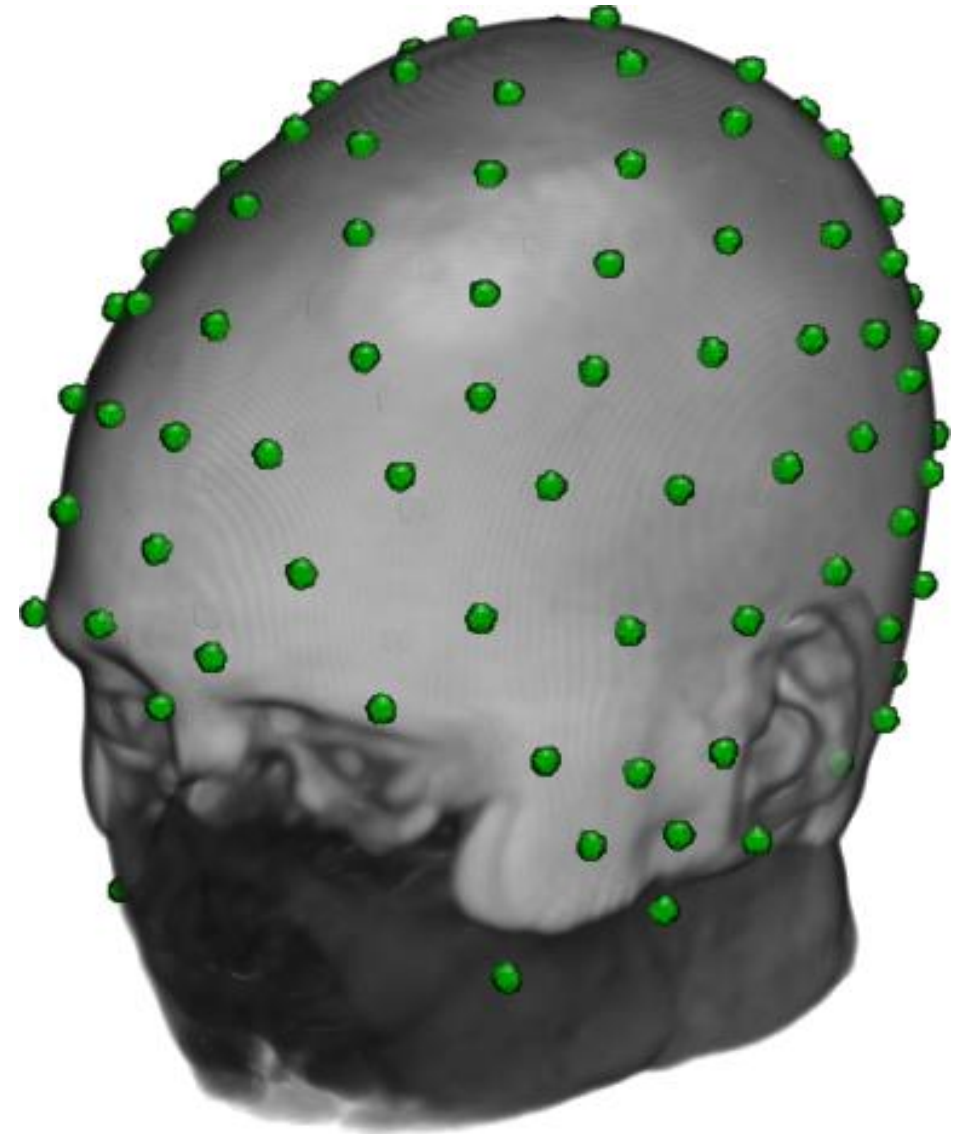


Figure 2. Regions of Interest (ROIs) shown on a 14 Year Old MRI

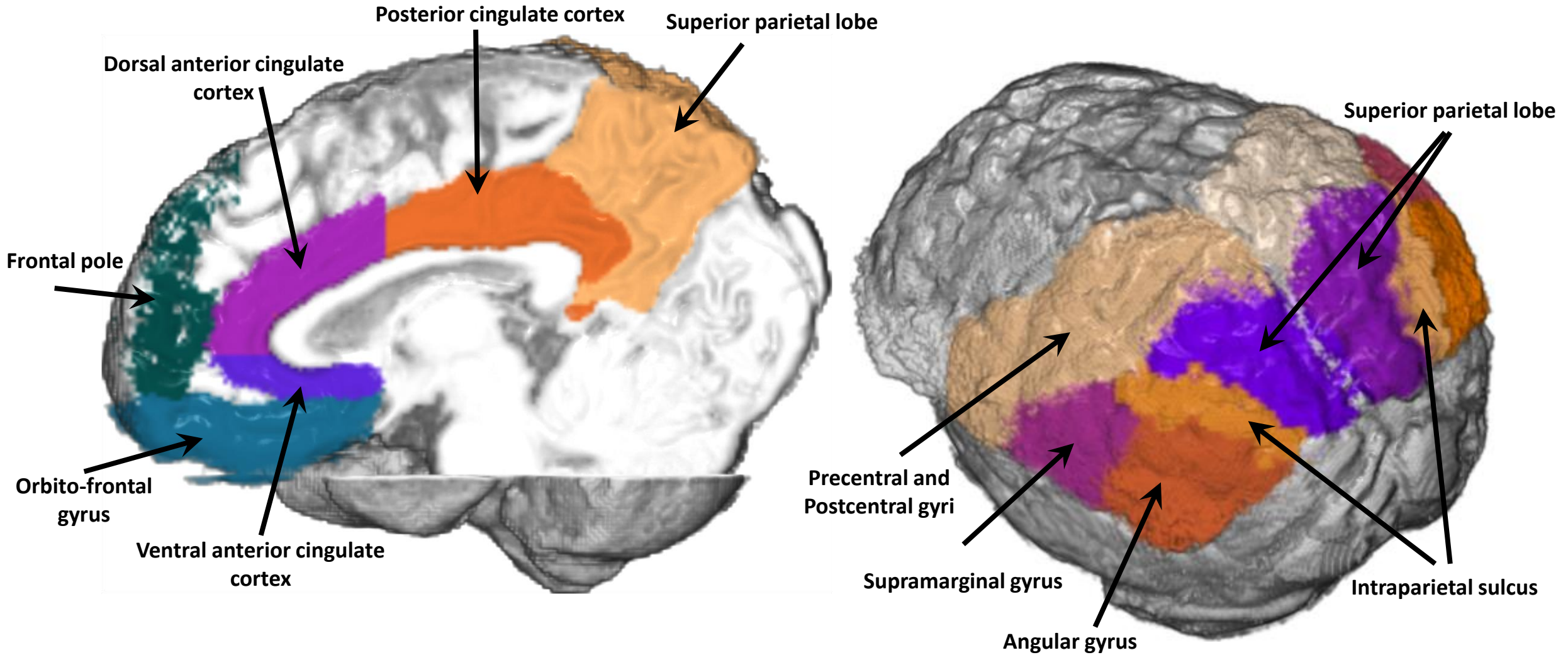
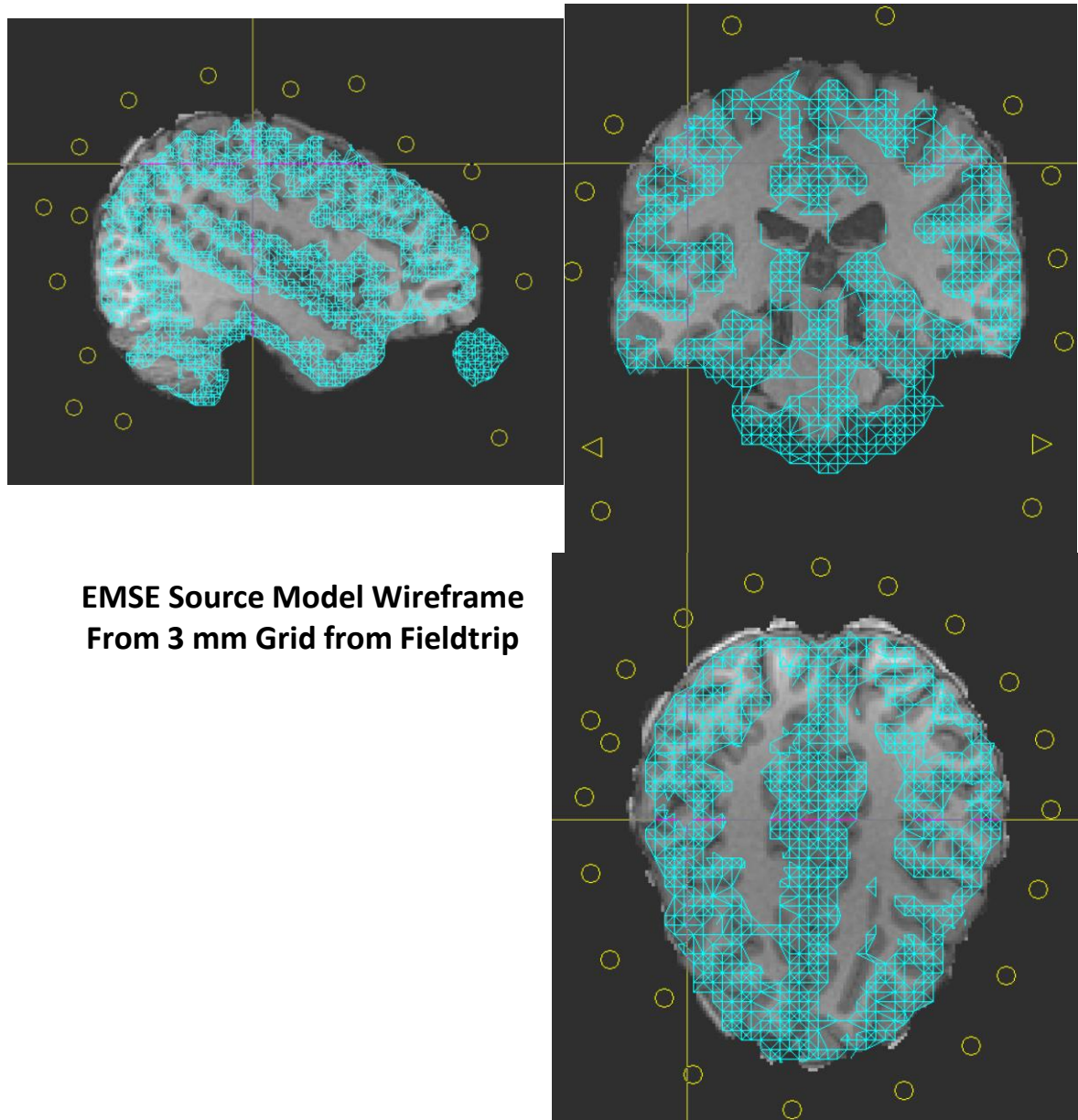
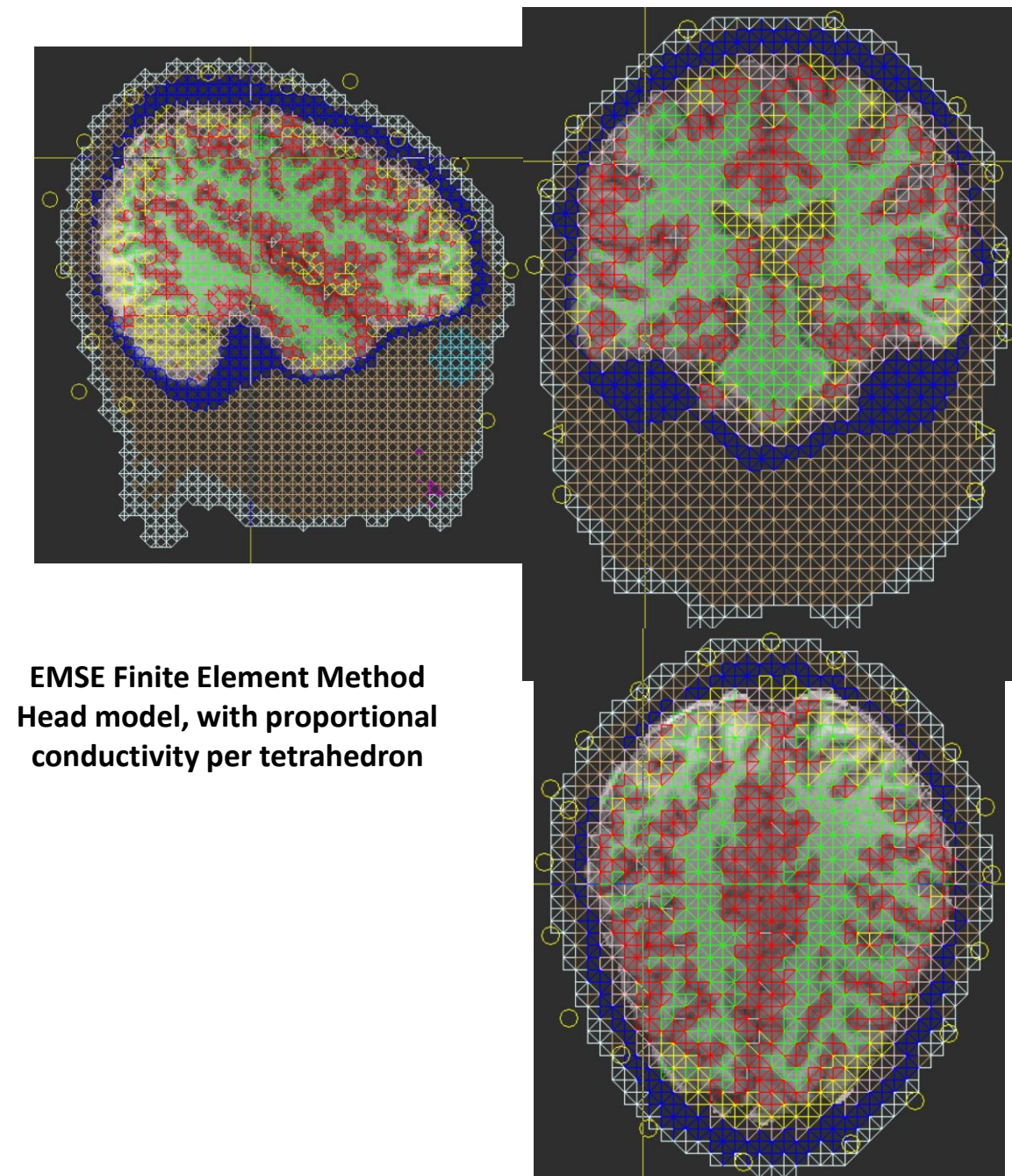


Figure 3. EMSE Source model and Finite Element Method (FEM) Head model



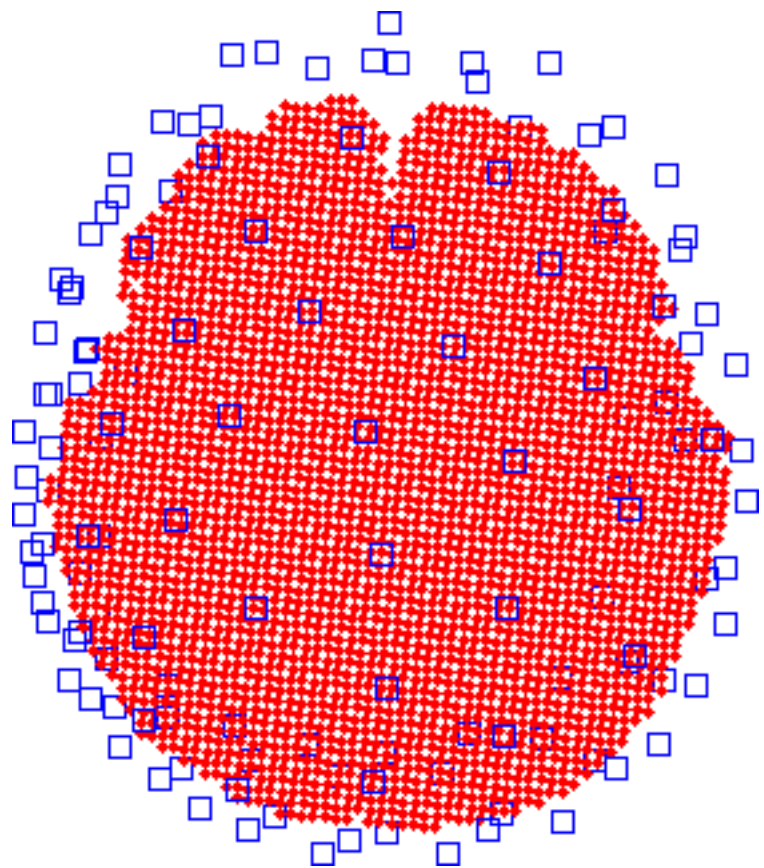
**EMSE Source Model Wireframe
From 3 mm Grid from Fieldtrip**



**EMSE Finite Element Method
Head model, with proportional
conductivity per tetrahedron**

Figure 4. The Fieldtrip source model, 2mm grid, with HGSN128 electrode locations

Axial view



Side projection

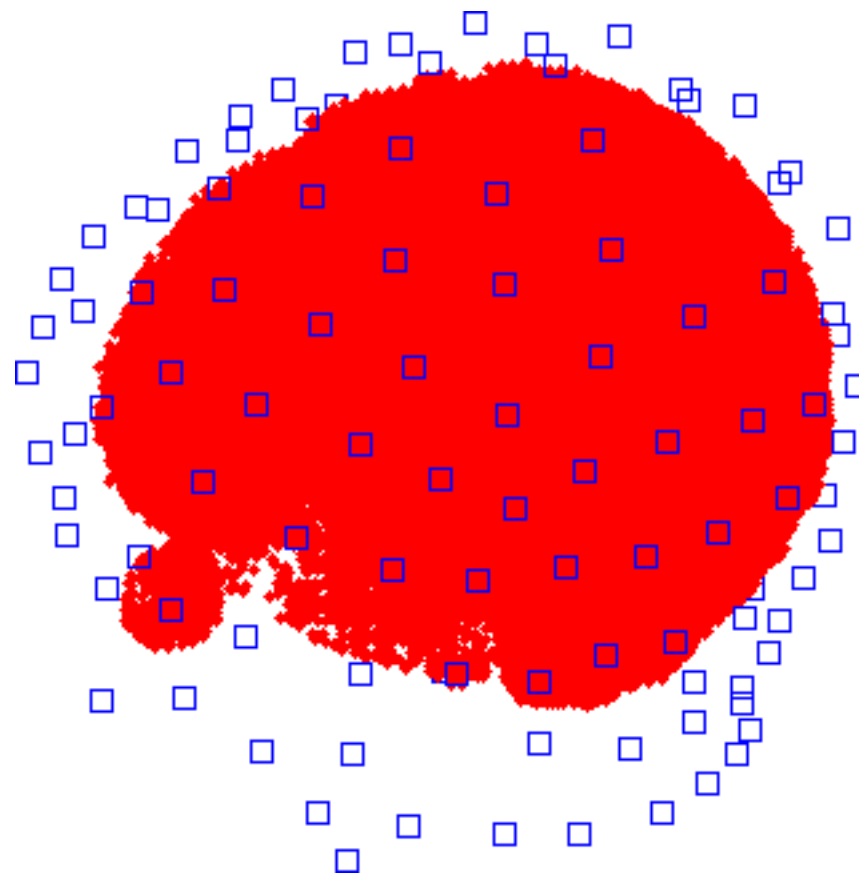
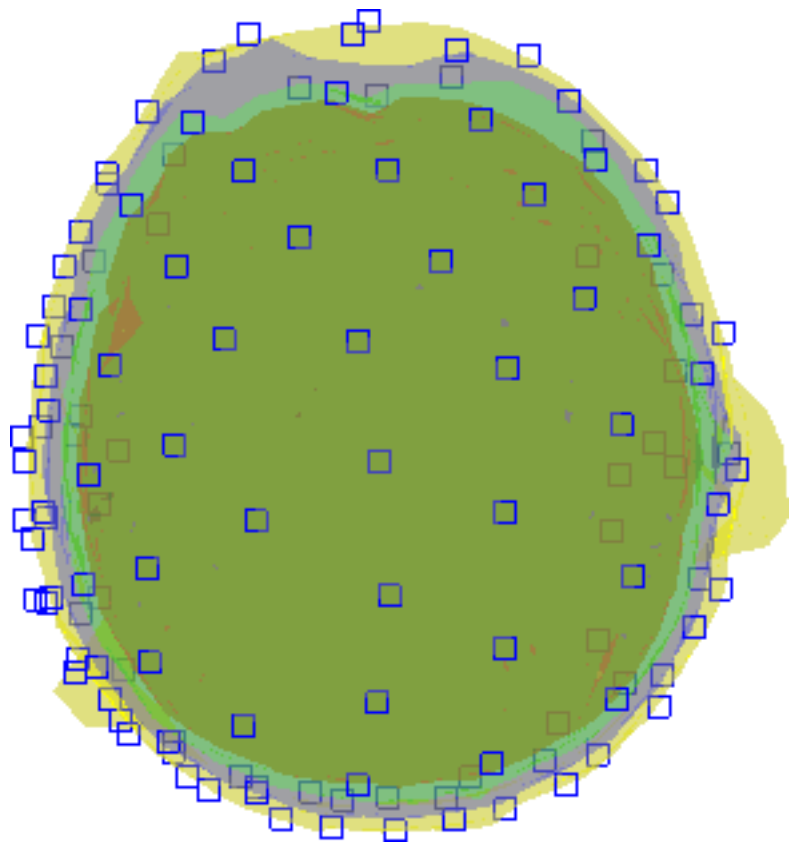


Figure 5. The Fieldtrip BEM (Boundary Element Method) Head mesh, with HGSN 128 electrodes

Axial view



Side projection

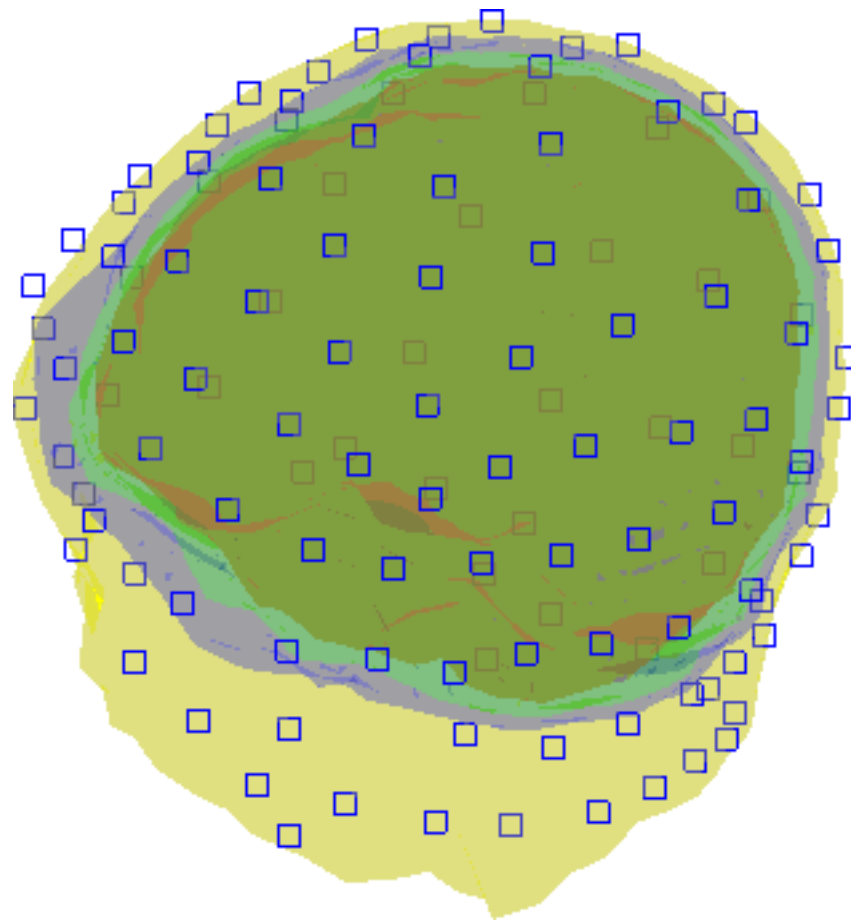
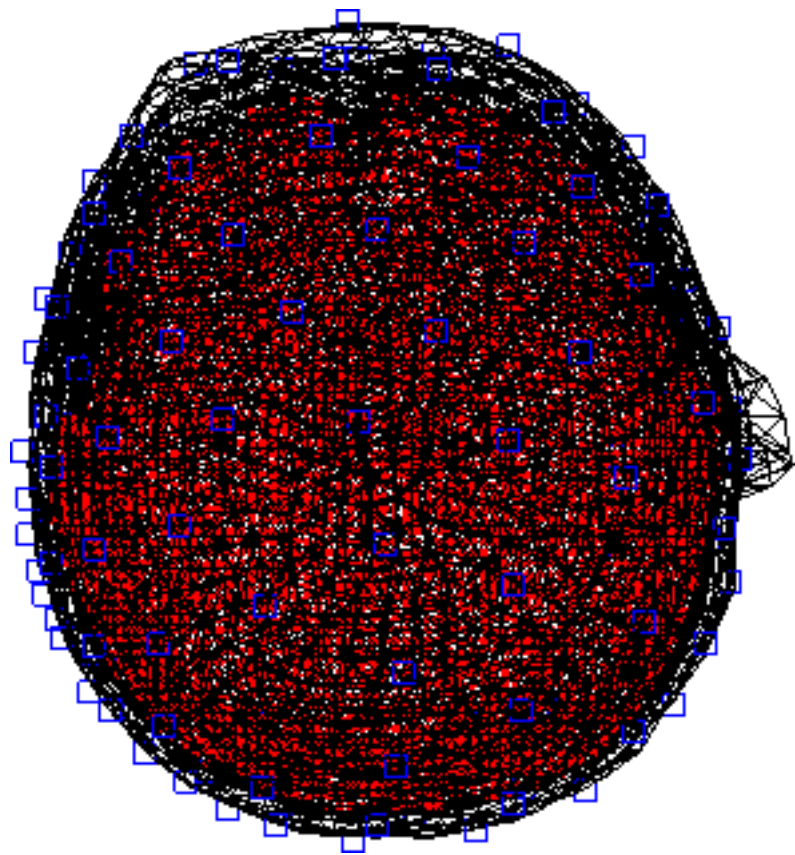


Figure 6. The Fieldtrip BEM (Boundary Element Method) Head model from DIPOLI methods, with HGSN 128 electrodes

Axial view



Side projection

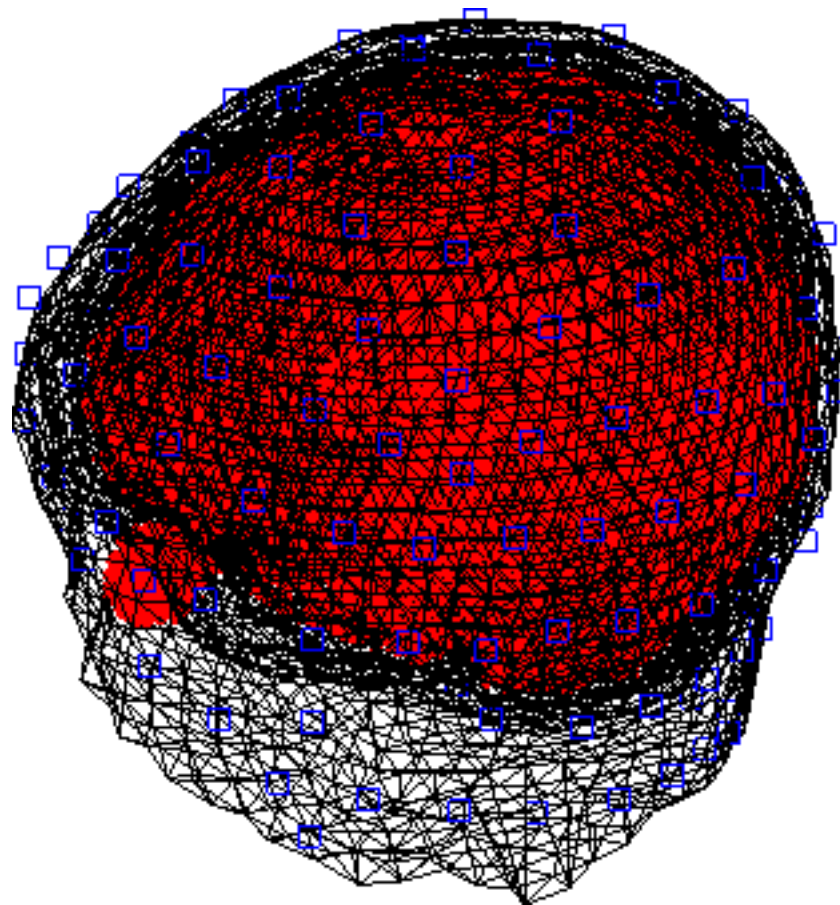
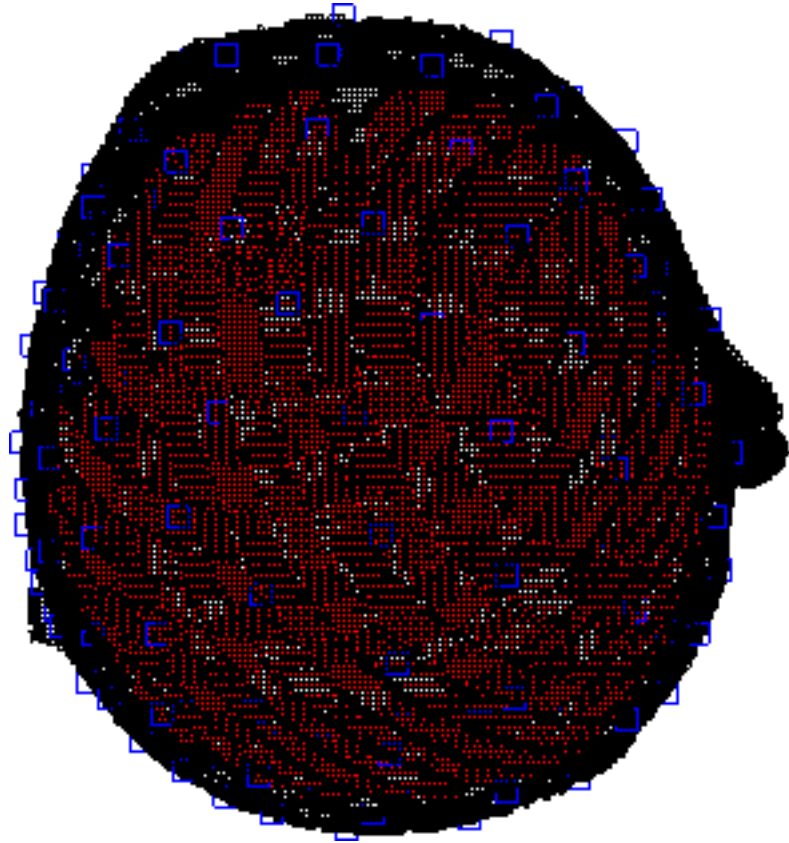


Figure 7. The Fieldtrip FEM (Finite Element Method) Head model from SIMBIO methods, with HGSN 128 electrodes

Axial view



Side projection

